Colloid and Polymer Science (2023) 301:989–999
https://doi.org/10.1007/s00396-023-05124-y

ORIGINAL CONTRIBUTION

Aggregation and disaggregation of Al_2O_3 nanoparticles: influence of solution pH, humic acid, and electrolyte cations

Tao Hu[1,2] · Weichuan Xu[1] · Dong Li[1] · Song Wang[1] · Yuxiang Wang[1] · Caijin Wu[1] · Liqiang Tan[1,2]

Received: 2 February 2023 / Revised: 11 May 2023 / Accepted: 15 May 2023 / Published online: 22 May 2023
© The Author(s), under exclusive licence to Springer-Verlag GmbH Germany, part of Springer Nature 2023

Abstract

Extensive use of Al_2O_3 nanoparticles in consumer and industrial products has led to concerns about their potential environmental impacts in the recent years. In most studies concerning Al_2O_3 aggregation and disaggregation, more was to consider the single factor that influences their environmental behaviors. Understanding the combined abiotic factors that influence the fate, transport, and stability of nanoparticles in a complex aquatic system has become extremely important. Here, we reported and analyzed the major abiotic factors such as typical solution pH, electrolyte cations in different valences (Na^+ and Ca^{2+}), and the presence of humic acid (HA) that influence the stability, aggregation, and disaggregation behaviors of Al_2O_3 nanoparticles in a complex aquatic system. Dynamic light scattering technique combined with fluorescence spectroscopic analysis was used to explore the aggregation mechanisms. Experimental results indicated that Al_2O_3 nanoparticle stability was mainly controlled by the steric hindrance, van der Walls, and electrostatic interactions between HA and Al_2O_3 nanoparticles. Aggregation kinetics and attachment efficiency studies induced by the addition of Na^+ and Ca^{2+} cations confirmed that divalent electrolytes could reduce the large energy barrier between the charged colloidal particles more efficiently, and induce a more aggressive aggregation of the particles. Additionally, the bridging effect of HA with Ca^{2+} was also an important mechanism for the aggregation enhancement, which had been confirmed by the fluorescence excitation-emission matrix (EEM) spectra analysis. These findings are useful in understanding the environmental challenges of inorganic colloidal particles in natural environments.

Keywords Al_2O_3 nanoparticles · Aggregation · Zeta potential · Size distribution

Introduction

In recent years, metal oxide nanoparticles, including nano-sized Fe_2O_3, ZnO, Al_2O_3, TiO_2, MgO, and CeO_2, had been developed and applied extensively in a number of different areas including electronics, cosmetics, energy technologies, and biomedical, catalytic, and material applications, as well as environmental remediation [1–3]. The use of metal oxide nanoparticles had seen exponential growth in consumer and industrial products [4–6]. Among the major types of manufactured nanoparticles, aluminum oxide (Al_2O_3), one of the most abundantly manufactured metal oxides on a nanoscale, had been widely used in high-performance ceramics, cosmetic fillers, packing materials, polishing materials, semiconductor materials, paints, composite materials, and resins [7–9]. The global production of Al_2O_3 has been increasing year after year, and it is more economically favorable to use [10–12].

The extensive use of Al_2O_3 nanoparticles in consumer and industrial products has led to concerns about their potential environmental impacts during recent years [13, 14]. Firstly, if Al_2O_3 nanoparticles were released into water systems, these particles could potentially cause harm to aquatic organisms including algae species and aquatic invertebrates [15]. Moreover, there was concern over the possible adverse effects of Al_2O_3 nanoparticles on human health. Many existing researches indicated that Al_2O_3 nanoparticles exhibited adverse effects on cell proliferation and cell viability in human lung epithelial cells and A549 carcinoma

✉ Liqiang Tan
tanliqiang@hyit.edu.cn

[1] National & Local Joint Engineering Research Center for Mineral Salt Deep Utilization, Huaiyin Institute of Technology, Huaian 223003, People's Republic of China

[2] Jiangsu Provincial Key Laboratory of Palygorskite Science and Applied Technology, Huaian 223003, People's Republic of China

cells through the biological and food cycle [16]. Understanding the aggregation and colloidal stability of manufactured Al_2O_3 nanoparticles in natural waters is essential to accurately evaluate their toxicity on aquatic organisms and human health [17–19]. Thus, investigations on the stability, migration, and aggregation propensity of Al_2O_3 nanoparticles in aquatic environments are of great significance.

To a certain degree, the particle diameter range of nanoparticles is an important parameter that determines their transport behavior, toxicity, and ultimate environmental fate in the water environment [20, 21]. According to the report, nanoparticle stability in aqueous environments depends on many parameters, including the environmental conditions (solution pH, ionic strength, and presence of other chemical compounds), nanoparticle concentration, and the nanoparticle intrinsic and surficial characteristics [22–24]. The unintended impact in aquatic environments, chemical reactivity, environmental fate, and behavior of nanoparticles and their possible interaction with environmental elements is thus a key issue in aquatic environmental risk assessment [25]. Therefore, this novel study investigates the aggregation and disaggregation behaviors of Al_2O_3 nanoparticles in different experimental conditions. In this paper, solution pH, electrolyte cations in different valences (Na^+ and Ca^{2+}), and humic acid (HA) were identified as major abiotic factors influencing the stability, aggregation, and disaggregation behaviors of Al_2O_3 nanoparticles in a complex aquatic system. In addition, dynamic light scattering (DLS) analysis was performed to explore the aggregation behaviors of Al_2O_3 nanoparticles and fluorescence spectra analysis was used to analyze the aggregation mechanisms. Information obtained in this study will be of fundamental significance for the understanding of the ultimate fate of inorganic colloids themselves and contaminants in complex environmental conditions [26].

Materials and methods

Materials

NaCl, $CaCl_2$, NaOH, HNO_3, and Al_2O_3 nanoparticles were obtained from commercial supplies (Shanghai Aladdin Biochemical Technology Co., Ltd.) and used without further purification. According to the manufacturer's data, the physical characteristics of Al_2O_3 nanoparticles are as follows: purity > 99%, diameter = 50 nm, and crystalline phase of approximately 30%γ versus 70%θ. Commercial HA with purity > 90% was purchased from Sinopharm Chemical Reagent Co., Ltd. and used with prior separation and purification according to our previous work [27]; C (50.15%), H (4.4%), O (39.56%), S (0.49%), and N (5.38%) were the main components in the sample. Analytical reagent grade chemicals (NaCl, $CaCl_2$, NaOH, and HNO_3) were used along with ultra-high-purity water (18.2 MΩ cm^{-1}), which was purified with a Milli-Q equipment and used throughout the experiments to prepare solutions. Al_2O_3 colloidal particles were diluted to the desired concentrations with deionized Milli-Q water prior to use as a research object to study the aggregation and disaggregation behaviors of inorganic colloids [28]. Stock solutions of NaCl and $CaCl_2$ were used as electrolytes to control the ionic strength of the solution and to study the effect of cation type on the stability of Al_2O_3 nanoparticles. An amount of 50 mg of purified HA was dissolved in 1L of Milli-Q water. The solution was then filtered over a 0.01-µm filter to remove all non-dissolved aggregates. The pH values of the solutions were adjusted by the addition of 0.01 M NaOH and/or HNO_3 to obtain the desired pH conditions.

Zeta potential and hydrodynamic diameter measurement

The zeta potential and hydrodynamic diameter measurements of aggregating Al_2O_3 nanoparticles were performed with a Zetasizer nanoseries (Malvern Nano-ZS, Malvern, UK) instrument. In the experiment, He–Ne laser was used as a coherent source of monochromatic radiation at 633 nm and the scattering angle was 173° for all measurements [29]. For the aggregation experiment, the achieved solution with a certain concentration range of HA and Al_2O_3 nanoparticles was immediately placed in a disposable polystyrene cuvette to track the average diameter variation trend of the particles. Similar experimental procedure was also conducted to obtain the aggregation behaviors of Al_2O_3 nanoparticles in the presence of different metal cations (Na^+ and Ca^{2+}). During the initial aggregation process, each autocorrelation function was accumulated for 15 s, and the whole process lasted 4500 s. All the experiments were performed in triplicates and average values were presented in the work.

Fluorescence measurements

The fluorescence excitation-emission matrix (EEM) spectra and emission intensity changes of HA were measured on a HITACHI F-7000 spectrofluorometer with a 450W Xenon lamp. The emission wavelengths were set from 200 to 900 nm, while the excitation wavelengths were set from 200 to 600 nm with scanning number 25 and increment 10 nm [30]. For all the above fluorescence measurements, the excitation and emission slit widths were set at 5.0 nm with a scan speed of 1200 nm/min.

Results and discussion

Influence of pH on surface properties and stability of Al_2O_3 nanoparticles and HA

The surface charge modifications and stability of Al_2O_3 nanoparticles caused by adjusting the solution pH were determined using pH titration curves at 0.001 M $NaNO_3$ ionic strength. As shown in Fig. 1A, there was an excellent relationship between the stability of Al_2O_3 nanoparticles and their electrophoretic properties. Meanwhile, the regularity of Al_2O_3 particles with different particle sizes being obtained by changing the pH value of the suspension can really reflect the dispersion and deposition of the aqueous suspensions of Al_2O_3 nanoparticles. As can be seen from Fig. 1A, the zeta potential values of Al_2O_3 nanoparticles were positive (30 ± 3.0 mV) and almost remained constant from pH 2.0 to 6.0, whereas the particles stayed the same size (220 ± 3 nm) through the entire pH range, which was larger than the original particle size (50 nm) of commercial Al_2O_3 particles, indicating an obvious aggregation of the colloidal particles in water solution [27]. Then, as the solution pH increased, the zeta potential value decreased to the point of zero charge (pH_{PZC}) at a pH about 9.4 ± 0.1, whereas the particle size increased rapidly and the highest value of the *z*-average diameter obtained for the particle was 1700 nm at the pH_{PZC}, which indicated a very easy and efficient aggregation of the particles when the positively charged surface was neutralized at $6.0 < pH < 9.4$ [31]. By further increasing the pH, the magnitude of the zeta potential decreased as the pH increased and reached a minimum value of about – 36 mV at pH of approximately 12.0. Over the pH range $9.4 < pH < 12.0$, one could also find that the particle size started to decrease rapidly and finally reached 220 ± 3 nm at pH 12.0 (it was similar to

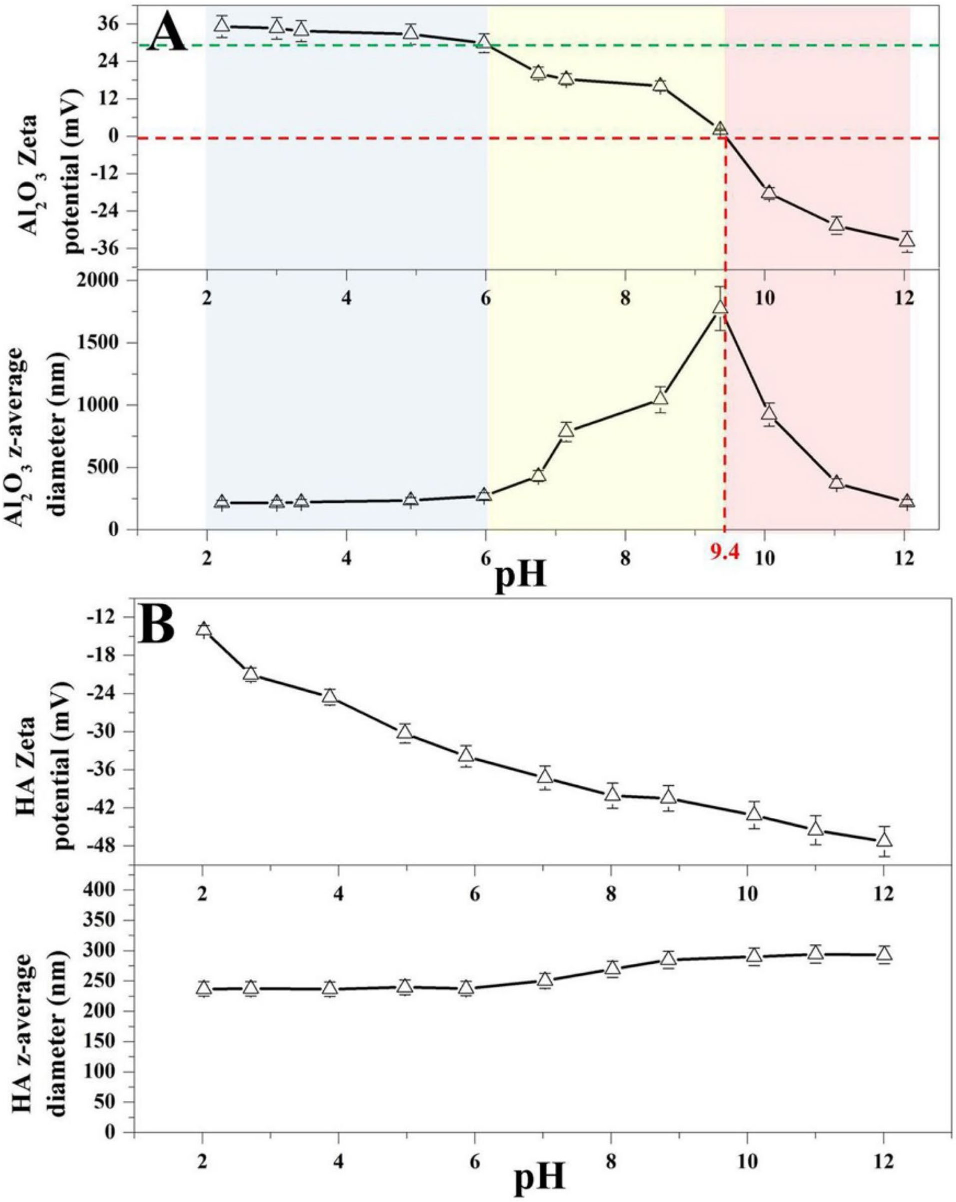

Fig. 1 Zeta potential variation and *z*-average diameter changes of Al_2O_3 particles (**A**) and HA molecules (**B**) as a function of pH. $C_{Al_2O_3} = 100$ mg/L, $C_{HA} = 50$ mg/L

the initial particle size at pH 2.0 to 6.0), which was due to the amphoteric nature of Al_2O_3 nanoparticles [32]. Al_2O_3 was easier to dissolve gradually at high pH, and there was a relationship between the dissolution behavior and the decrease of the particle size.

The variations of the zeta potential of HA (50 mg/L) under different pH conditions were determined in a stock solution of $NaNO_3$ to produce a background electrolyte concentration of 0.001 mol/L (Fig. 1B). Holding ionic strength constant, the zeta potential of HA decreased approximately linearly with increasing pH from − 14.0 mV at pH 2.0 to − 47.3 mV at pH 12.0, which was due to the existence of substantial amounts of carboxylic acid and phenolic functional groups on its surface [33]. To get an insight into a general trend of the aggregation properties of HA, the dependence of *z*-average on pH for HA at constant ionic strength (0.001 M $NaNO_3$) is also illustrated in Fig. 1B. The *z*-average diameter of HA molecules was measured to be ~ 236 nm under acidic conditions; however, with the increase of solution pH, a slightly larger aggregate size (~ 293 nm) could be observed at pH > 8, which was because HA exhibited more than one type of macromolecular structure in aqueous solutions under different pH conditions [34]. Under acidic conditions, the molecules of HA showed globular and ring-like structures with a smaller aggregate size; however, the molecules became linear and/or sheet-like structures as the pH increases [34, 35]. Therefore, a slightly larger aggregate size could be observed under alkaline conditions as presented in Fig. 1B. Experimental data obtained in this work were shown to be in good agreement with experimental values obtained in other works [35, 36].

Effect of HA on the stabilization of Al_2O_3 nanoparticles under different pH conditions

$pH < pH_{PZC, Al_2O_3}$ (pH = 6.0)

The surface properties and particle size distribution of Al_2O_3 nanoparticle aggregates in the presence of HA were determined at pH = 6.0 ($pH < pH_{PZC}$) to explore the capacities of HA in influencing the aggregation or stabilization of the particles. As shown in Fig. 2, before adding HA to the suspensions ($C_{HA} = 0$ mg/L), Al_2O_3 nanoparticles showed a highly positive zeta potential value of 30.0 mV and a *z*-average diameter of 293 nm. However, after the addition of HA, the concentration influence of HA on zeta potential and the *z*-average diameter distribution curves were classified into three critical regions. In the first region (blue area in Fig. 2, $C_{HA} = 0$–2.5 mg/L), the addition of HA led to a rapid increase in *z*-average diameter of Al_2O_3 nanoparticle aggregates. The zeta potential decreased with increasing HA concentration and reached the pH_{PZC} at the concentration of 2.5 mg/L. Additionally, the *z*-average diameter reached a maximum value of 2157 nm, which indicated that the charge neutralization mechanism was responsible for the formation of the large aggregates [37]. With the increase of HA concentration as presented in the second region (yellow area in Fig. 2, $C_{HA} = 2.5$–5.0 mg/L), it was established that charge inversion led to a significant decrease of the zeta potential and *z*-average diameter values until a HA mass concentration of 5.0 mg/L [38]. Finally, in the third region (red area in Fig. 2, $C_{HA} = 5.0$–10.0 mg/L), the nanoparticles were in a diameter of 239 nm, and had a negative zeta potential

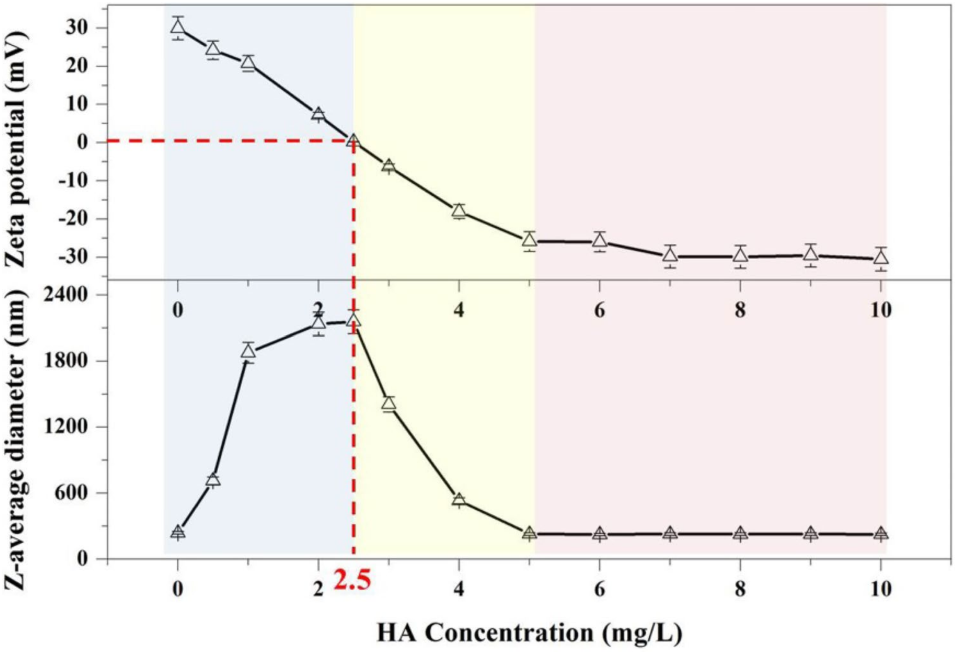

Fig. 2 The variations of zeta potential and *z*-average diameter of Al_2O_3 nanoparticles due to the presence of different concentrations of HA at pH 6.0. $C_{Al_2O_3} = 100$ mg/L

of − 30.5 mV, enough to keep the nanoparticles stable in aqueous solutions without aggregating. The system was close to stabilization again due to the addition of higher HA concentrations.

$pH = pH_{PZC, Al_2O_3}$ (pH = 9.4)

The zeta potential and *z*-average diameter values of HA were found to be − 41.0 ± 2.0 mV and 290 ± 5 nm at pH = 9.4, respectively (Fig. 1B). However, as shown in Fig. 3, after the addition of HA, the system remained at equilibrium for a substantial amount of time (4500 s) between each measurement. We observed a rapid decrease in zeta potential of Al_2O_3 nanoparticles until a plateau at around − 32 mV when HA concentration was increased to 3 mg/L or greater during the negative surface charging process. Also, note that in this process, the fragmentation of the Al_2O_3 nanoparticles became significant, and the *z*-average diameter decreased and maintained at ~ 400 nm when HA concentration was in excess of 3 mg/L.

The kinetics of disaggregation of Al_2O_3 nanoparticles at pH = 9.4 was also measured as a function of time and HA initial concentration. The extent of the nanoparticle disaggregation was characterized by the variation of the zeta potential and *z*-average diameter values in all experiments. As shown in Fig. 4, the kinetic measurements revealed that the zeta potential and *z*-average diameter of Al_2O_3 nanoparticles decreased with the increase of HA concentration until one steady count at last. Typical rate curves with two different regimes for the aggregation of Al_2O_3 nanoparticles could be observed; the rate of disaggregation was comparatively high only during the initial period and decreased considerably later. Additionally, as can be seen, increasing HA initial concentration caused a larger amount of Al_2O_3 nanoparticles to disaggregate, and the maximum disaggregation was obtained at ≥ 7 mg/L HA with a final *z*-average diameter at 625 nm, which was a little larger than the initial Al_2O_3 particle size (293 nm), indicating a partial disaggregation of the nanoparticles [39]. The rapid decrease of zeta potential values of Al_2O_3 nanoparticles after the addition of HA indicated that the adsorption of negatively charged HA on Al_2O_3 nanoparticle surface resulted in a high electrostatic repulsion between Al_2O_3 nanoparticles, thus leading to a disaggregation of the nanoparticles [40].

$pH > pH_{PZC, Al_2O_3}$ (pH = 11.0)

As shown in Fig. 5, the addition of HA caused a significant decrease in the zeta potential values at pH 11.0. However, there was a slight increase in the average size of the Al_2O_3 nanoparticles as HA concentration increased. Such experimental results showed that the adsorption of HA on Al_2O_3 nanoparticles was limited, and the effect of non-electrostatic van der Walls interactions played a significant role between HA and Al_2O_3 nanoparticles at $pH > pH_{PZC, Al2O3\ (pH\ =\ 11.0)}$ [41].

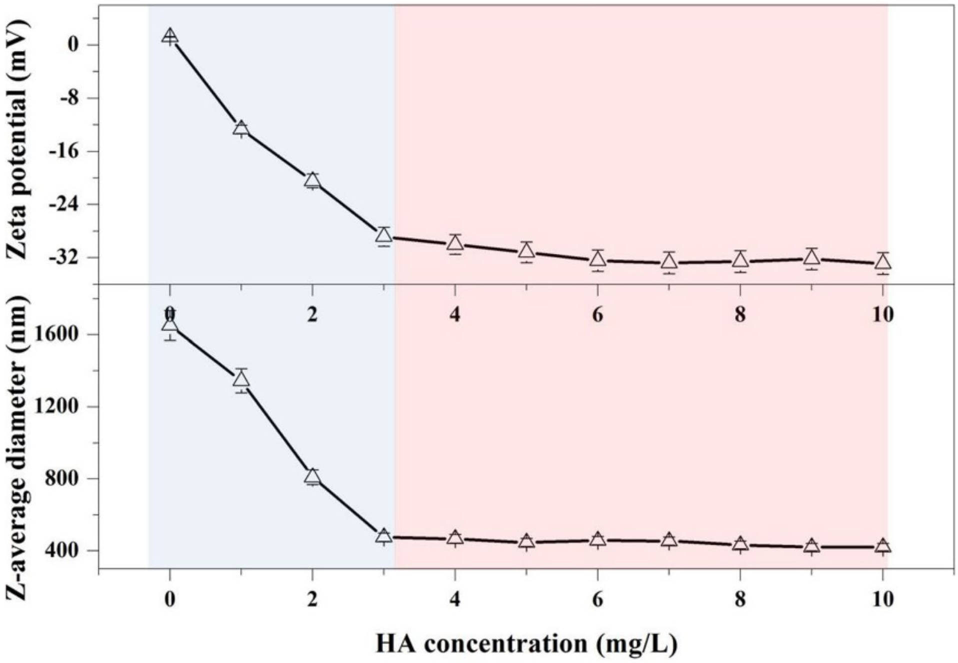

Fig. 3 The variations of zeta potential and *z*-average diameter of Al_2O_3 nanoparticles due to the presence of different concentrations of HA at pH 9.4. $C_{Al_2O_3} = 100$ mg/L

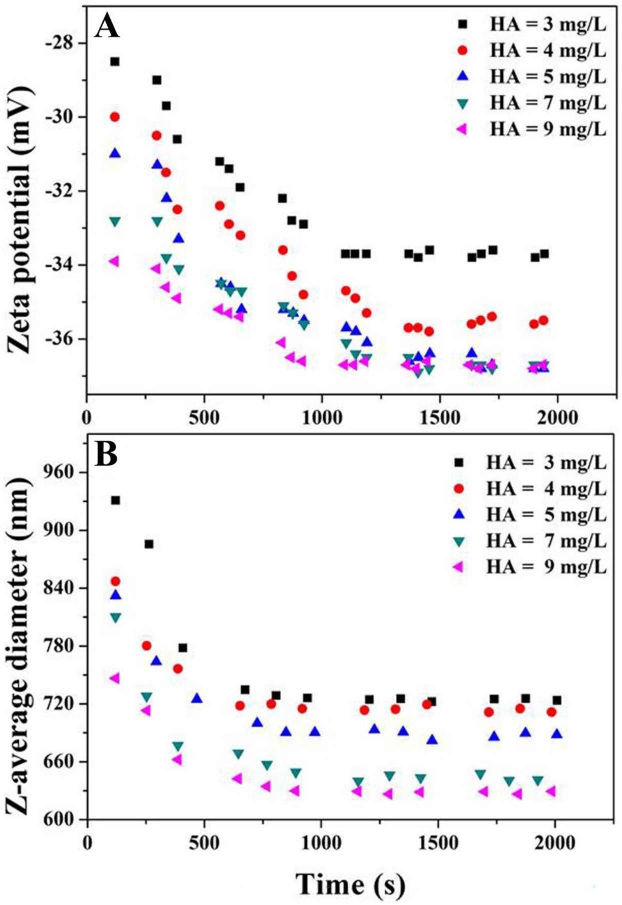

Fig. 4 **A** Time-dependent variation of the zeta potential of Al_2O_3 nanoparticles under different HA concentrations. **B** The extent of disaggregation of Al_2O_3 nanoparticles as a function of time at several HA concentrations. $pH = pH_{pzc}$. $C_{Al_2O_3} = 100$ mg/L

Electrolyte-dependent aggregation behavior of Al_2O_3 nanoparticles

Aggregation kinetics and attachment efficiency studies

To examine the potential effects of electrolyte species on the aggregation of Al_2O_3 nanoparticles in the presence of HA, the aggregation kinetics and *z*-average diameter changes of Al_2O_3 nanoparticles were quantified in aqueous suspensions containing either monovalent (Na^+) or divalent cations (Ca^{2+}) as a background electrolyte through a combination of batch and column experiments. In the presence of Na^+, an increase of the electrolyte concentration to 10 or 12 mM led to a rapid aggregation of the Al_2O_3 nanoparticles (Fig. 6A). However, further increase of the Na^+ concentration over 12 mM had a weak effect on the enhancement of aggregation rate. But for the divalent electrolyte, a much lower Ca^{2+} concentration could induce a rapid aggregation of the particles; Ca^{2+} was far more effective in inducing Al_2O_3 nanoparticle aggregation. For instance, in the presence of 0.2 mM Ca^{2+}, Al_2O_3 nanoparticles could quickly aggregate and finally reached a *z*-average size of ~ 1000 nm as presented in Fig. 6B, while the same aggregate size of the particles due to the presence of Na^+ could be obtained at a much higher concentration of 10 mM as shown in Fig. 6A. As expected, divalent cations could make the surface charge of Al_2O_3 nanoparticles less negative due to the higher charge screening effect, which was beneficial for aggregation and thus inducing aggregation at a much lower concentration as compared to monovalent ions [41–44].

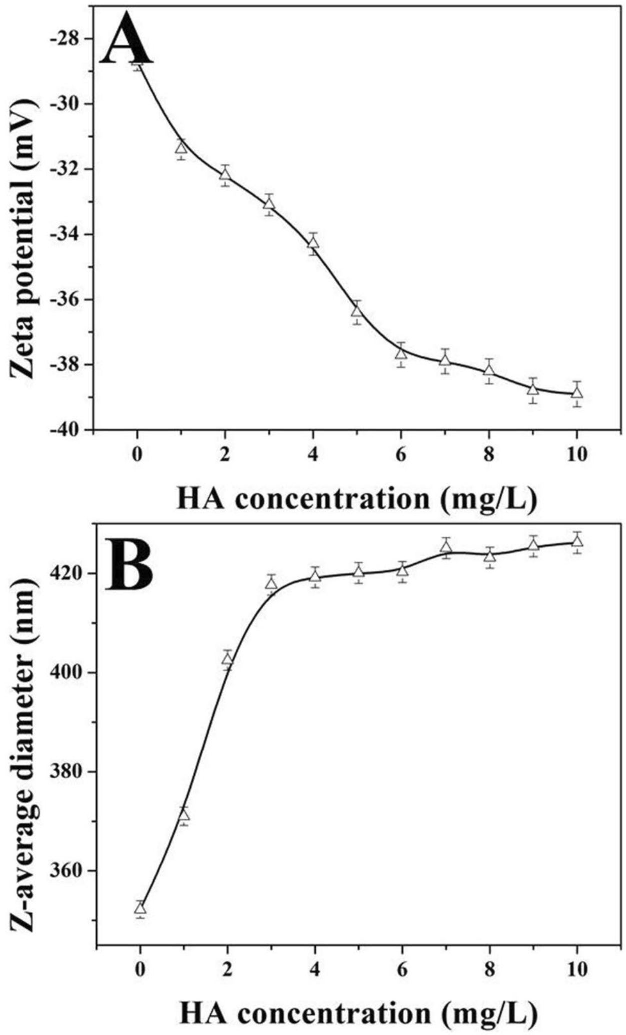

Fig. 5 The variations of zeta potential and *z*-average diameter of Al_2O_3 nanoparticles due to the presence of different concentrations of HA at pH 11.0. $C_{Al_2O_3} = 100$ mg/L

The Al_2O_3 nanoparticle attachment efficiency was determined from the aggregation kinetic profiles for Na^+ and Ca^{2+} electrolyte species (Fig. 6C). For Na^+ electrolyte, the attachment efficiency increased with the increase of electrolyte concentration until the Na^+ concentration reached the critical coagulation concentration (CCC), which represented

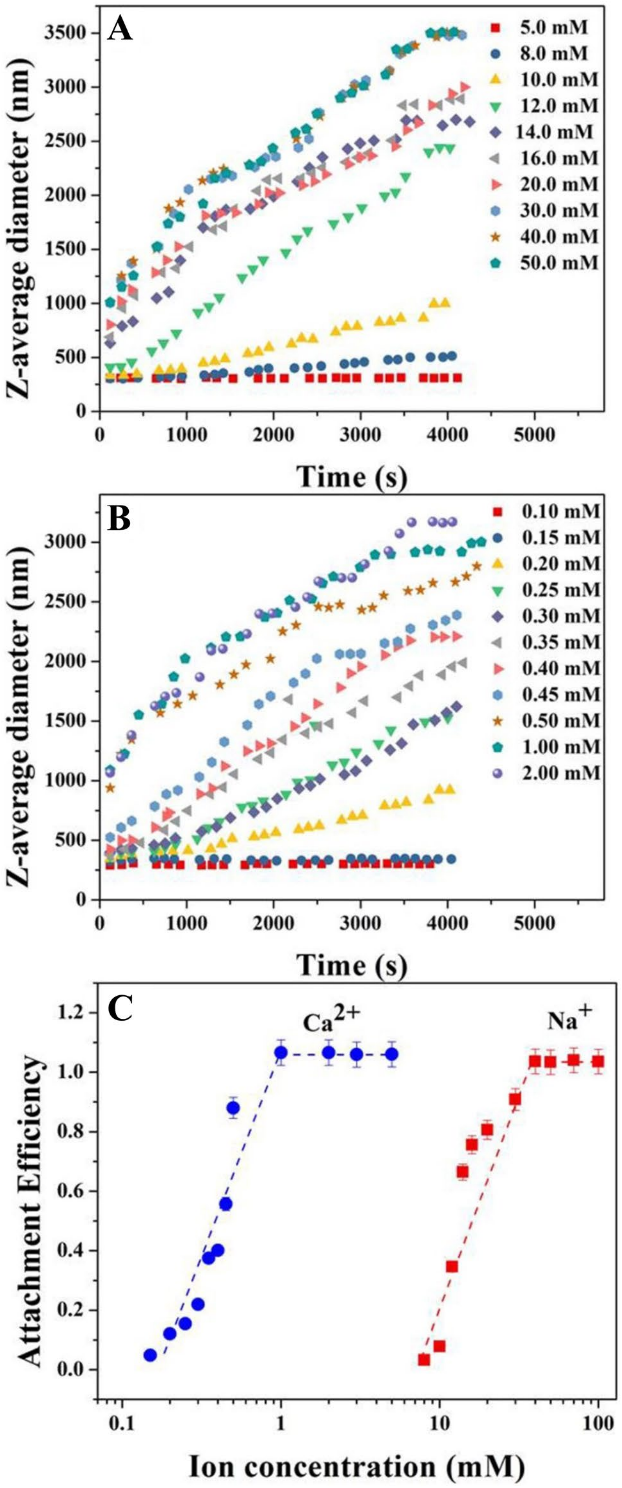

Fig. 6 Aggregation profiles (**A**, **B**) and attachment efficiency studies (**C**) of Al_2O_3 nanoparticles as a function of Na^+ (**A**) and Ca^{2+} (**B**) electrolyte concentration. C_{HA} = 6 mg/L, pH = 6.0

the minimum concentration of electrolyte that was needed to induce the occurrence of the aggregation [45]. In the presence of Na^+, CCC value determined here for Al_2O_3 nanoparticles was about 40 mM. As the concentration of Na^+ continued to increase, the negative surface charge of Al_2O_3 nanoparticles weakened significantly in the reaction-limited regime, thereby decreasing the electrostatic repulsion between particles and enhancing the attachment efficiency values [46]. When the Na^+ concentration exceeded 40 mM, an increase in Na^+ concentration had no effect on attachment efficiency. Under these conditions, the electrostatic repulsion between Al_2O_3 nanoparticles was completely suppressed and every collision between nanoparticles resulted in attachment [47]. In the presence of Ca^{2+}, the curve for Al_2O_3 nanoparticle attachment efficiency was quite similar to the regime due to the addition of Na^+, except that the CCC for divalent Ca^{2+} (0.5 mM) was much lower than that for Na^+ (40 mM). Experimental results of CCC values obtained in this work have stated that multivalent ions were more effective in reducing the energy barrier between Al_2O_3 nanoparticles, and therefore promoting a more aggressive colloidal aggregation than monovalent ions.

Fluorescence spectra analysis

With the kinetic experiments indicating differences in aggregation mechanisms of Al_2O_3 nanoparticles in the presence of HA and different electrolyte species, comparing the fluorescence EEM spectra changes of HA due to the addition of electronic ions of Na^+ and Ca^{2+} in Al_2O_3 suspensions can provide more insights into the respective aggregation mechanisms.

In order to obtain the optimum fluorescence spectra analytical conditions, the sorption experiment of HA on Al_2O_3 nanoparticles as a function of pH and HA concentration was investigated firstly in Fig. 7. It was observed that the sorption of HA on Al_2O_3 was highly dependent on solution pH and favored at lower pH values due to the electrostatic attractive interactions. In the case of C_{HA} = 5 mg/L, pH < 9.0, the sorption percentage can be up to 99.5%, which indicated that HA was almost all adsorbed on the surface of Al_2O_3 nanoparticles. Therefore, according to the results of the sorption experiment, the optimum fluorescence spectra analytical conditions (pH = 7.0, C_{Na^+} = 40 mM, $C_{Ca^{2+}}$ = 0.5 mM, C_{Al2O3} = 100 mg/L, C_{HA} = 5 mg/L) were determined as presented in Fig. 8.

The EEM spectra of HA (Fig. 8A) and HA aggregates with the presence of electronic ions of Na^+ and Ca^{2+} are shown in Fig. 8B and C, respectively. In Fig. 8A, two obvious fluorescent components were distinguished, including one carboxylic-like fluorophore (peak 1, excitation/emission = 250–275/425–475 nm), and one phenolic-like fluorophore (peak 2, excitation/emission = 300–325/425–450 nm) [48]. Additionally, the emission intensity maxima corresponding to peak 1 and 2 are listed in Fig. 8D as a comparison. Similar EEM contour plot

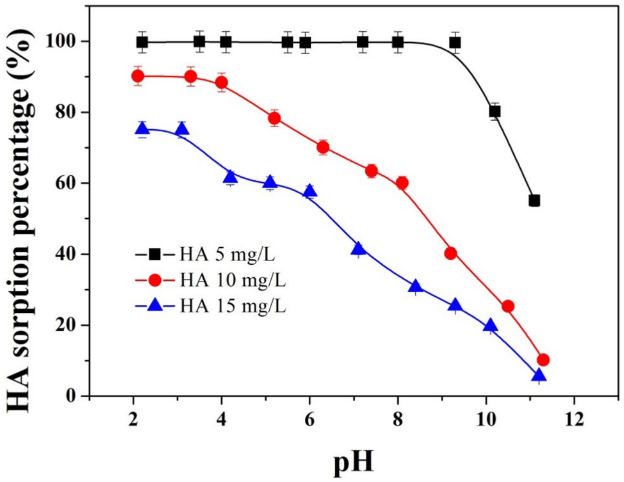

Fig. 7 The influence of pH on the sorption of HA with varying concentrations on Al_2O_3 nanoparticles. $C_{Al_2O_3} = 100$ mg/L, $I = 0.01$ mol/L $NaNO_3$

of HA aggregates after the addition of Na^+ ions in the suspension could be obtained in Fig. 8B; only the emission intensities of peaks 1 and 2 suffered a slight decrease as presented in Fig. 8D. However, after the addition of Ca^{2+} in the suspension (Fig. 8C), peak 2 disappeared and the emission intensity of peak 1 was weakened from 116 to 53 a.u. as shown in Fig. 8D, which indicated that the complex could remarkably quench the emission intensity of HA, and carboxyl and phenolic hydroxyl groups were both very effective in binding Ca^{2+} ions [49]. The results indicated that the Al_2O_3 nanoparticles may aggregate by more than one aggregation mechanism due to the presence of metal ions in different valence states. In the presence of monovalent Na^+, increasing the ionic strength effectively suppressed the electrostatic double-layer repulsion; there was no repulsive energy barrier when two particles approached each other, and thus inducing the aggregation of Al_2O_3 nanoparticles. As for the divalent Ca^{2+}, Ca^{2+}

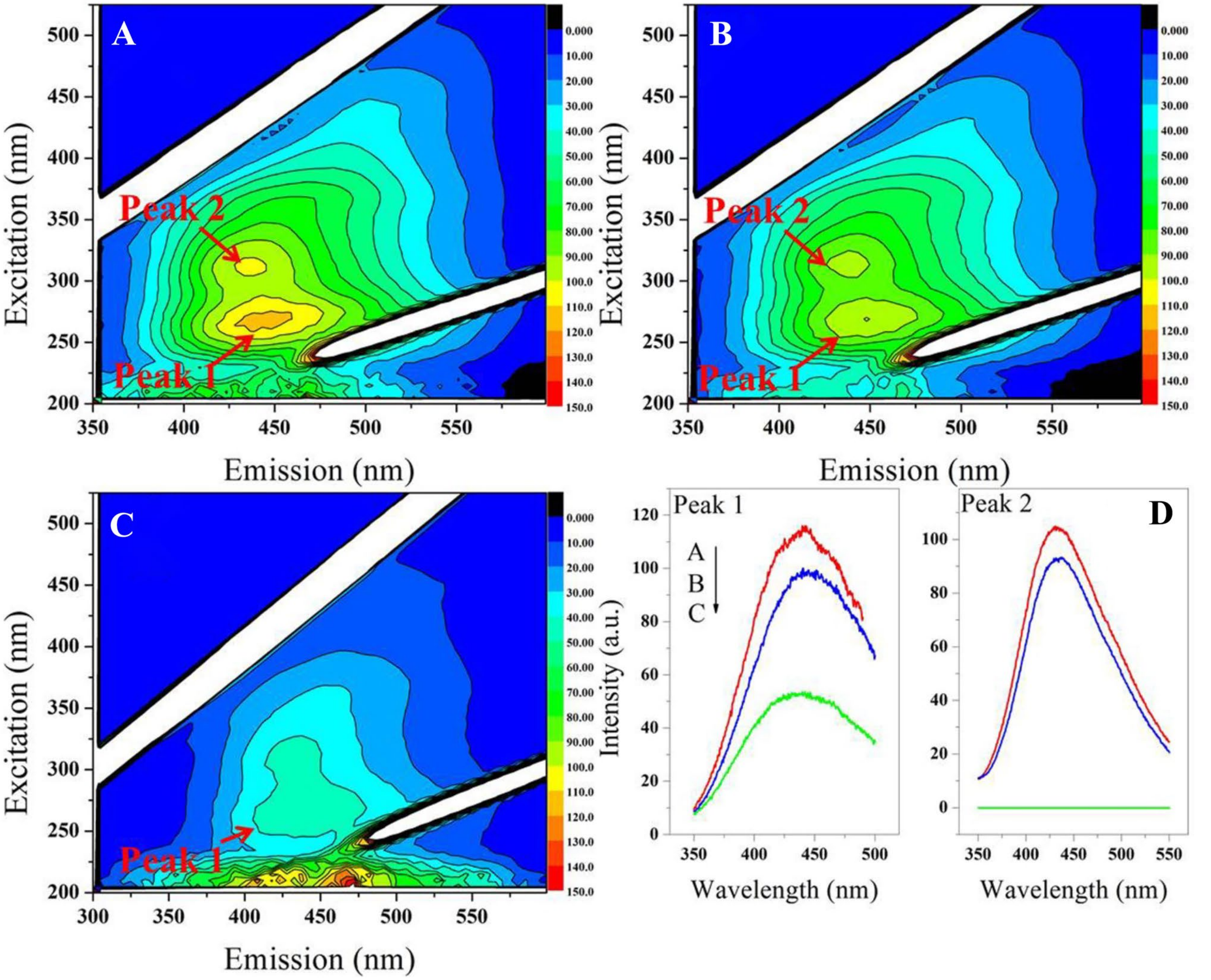

Fig. 8 Fluorescence EEM spectra of HA (**A**) and HA aggregates in the presence of Na^+ (**B**) or Ca^{2+} (**C**) metal ion at pH 7.0. $C_{Na^+} = 40$ mM, $C_{Ca^{2+}} = 0.5$ mM, $C_{Al_2O_3} = 100$ mg/L, $C_{HA} = 5$ mg/L. **D** Changes in the intensity of the emission spectra of peak 1 and peak 2

interacted with HA, whereas HA could be adsorbed on the surface of Al_2O_3 nanoparticles, and HA acted as a bridge between Ca^{2+} ions and Al_2O_3 nanoparticles. Therefore, the *z*-average diameter of Al_2O_3 nanoparticles could be increased through the function of complexing bridging between HA and Ca^{2+}, which in turn resulted in the enhancement of aggregation [50]. There is a good coherence between the potential mechanism and the fact that the mapping of calcium was well associated with the aggregate positions of Al_2O_3 nanoparticles.

Conclusions

The data presented here indicated that combined influencing factors such as solution pH, HA, and ionic strength had great impacts on the stability of Al_2O_3 nanoparticles in the water environment system. An efficient aggregation of the particles can be observed at $6.0 < pH < 9.4$ when the positively charged surface was neutralized. The largest aggregate size obtained at $pH = pH_{PZC}$ indicated there were close connections between the surface charge properties and stability of Al_2O_3 nanoparticles. The existence of the environmental aquatic concentration ranges of HA and electrolyte cations had great influence on the particle size, size distribution, and colloidal stability of Al_2O_3 nanoparticles. The complex behaviors of isolated or aggregated Al_2O_3 nanoparticles were dependent on the surface charge modification by adding different concentrations of HA in the suspension. From the theoretical point of view, the electrostatic interactions between the negatively charged surfaces made Al_2O_3 nanoparticles dispersed stably in the suspension at $pH > pH_{PZC}$. At $pH < pH_{PZC}$, the electrostatic adsorption of the negatively charged HA macromolecules onto the surface of positively charged nanoparticles induced charge neutralization, where the maximum aggregation was achieved. However, a relatively strong charge inversion could be observed after a further addition of HA in the suspension, which indicated disaggregation became significant due to electrostatic repulsions between Al_2O_3 nanoparticles. Aggregation kinetic measurements and fluorescence EEM spectra analysis indicated that divalent Ca^{2+} can make the surface charge of Al_2O_3 nanoparticles less negative due to the higher charge screening effect, and induce a rapid aggregation of the particles at a much lower concentration as compared to monovalent Na^+. The function of complexing bridging between HA and Ca^{2+} also resulted in the enhancement of aggregation. The Al_2O_3 nanoparticle stability was mainly controlled by the mechanism involving attractive and repulsive electrostatic interactions, van der Walls, steric effects, and the bridging effect of HA with electrolyte cations and nanoparticles. The study highlighted the influence of solution pH, HA, and electrolytes on the stability and colloidal aggregation process of metal oxide nanoparticles. These findings are useful in understanding the size change of the metal oxide nanoparticles, as well as the removal of the particles and HA from aqueous media, which is of great importance in assessing the environmental pollution of nanoparticles.

Acknowledgements The authors are thankful to the analysis and testing center of Huaiyin Institute of Technology.

Author contribution T.H., C.W., W.X., and S.W. conceived the study and performed the measurements. L.T., Y.W., and D.L. analyzed the results and prepared the manuscript.

Funding This work is financially supported by the Fundamental Research Funds for the Jiangsu Provincial Key Laboratory of Palygorskite Science and Applied Technology (HPK201806) and the Fundamental Research Funds for the National & Local Joint Engineering Research Center for Mineral Salt Deep Utilization (SF201905).

Data availability The datasets generated during the current study are available from the corresponding author on reasonable request.

Declarations

Conflict of interest The authors declare no competing interests.

References

1. Brayner R, Ferrari-IIiou R, Brivois N, Djediat S, Benedetti MF, Fiévet F (2006) Toxicological impact studies based on Escherichia coli bacteria in ultrafine ZnO nanoparticles colloidal medium. Nano Lett 6:866–870
2. Zhang M, Guiraud P (2013) Elimination of TiO_2 nanoparticles with the assist of humic acid: influence of agglomeration in the dissolved air flotation process. J Hazard Mater 260:122–130
3. Lu W, Lieber CM (2007) Nanoelectronics from the bottom up. Nat Mater 6:841–850
4. Ma R, Levard C, Judy JD, Unrine JM, Durenkamp M, Jefferson B, Lowry G (2014) Fate of zinc oxide and silver nanoparticles in a pilot wastewater treatment plant and in proceed biosolids. Environ Sci Technol 48:104–112
5. Hou L, Li K, Ding Y, Li D, Chen J, Wu X, Li X (2011) Removal of silver nanoparticles in simulated wastewater treatment processes and its impact on COD and NH_4 reduction. Chemosphere 12(42):248–252
6. Meyer DE, Curran MA, Gonzalez MA (2011) An examination of silver nanoparticles in socks using screening-level life cycle assessment. J Nanopart Res 13:147–156
7. Li M, Czymmek KJ, Huang CP (2011) Responses of Ceriodaphnia dubia to TiO_2 and Al_2O_3 nanoparticles: a dynamic nano-toxicity assessment of energy budget distribution. J Hazard Mater 187:502–508
8. Yiamsawas T, Mahian O, Dalkilic AD, Kaewnai S, Wongwises S (2013) Experimental studies on the viscosity of TiO_2 and Al_2O_3 nanoparticles suspended in a mixture of ethylene glycol and water for high temperature applications. Appl Energ 111:40–45
9. Zhu Y, Ong PP (2001) Thin films of silicon nanoparticles embedded in Al_2O_3 matrices. Surf Rev Lett 8(5):559–564
10. Laycock A, Stolpe B, Römer I, Dybowska A, Valsami-Jones E, Lead JR (2014) Rehkämper M., Synthesis and characterization of

isotopically labeled silver nanoparticles for tracing studies. Environ Sci: Nano 3:271–283

11. Pavasupree S, Ngamsinlapasathian S, Nakajima Y, Yoshikawa S (2006) Synthesis, characterization, photocatalytic activity and dye-sensitized solar cell performance of nanorods/nanoparticles TiO_2 with mesoporous structure. J Photoch Photobio A 184:163–169
12. Majedi SM, Lee HK (2016) Recent advances in the separation and quantification of metallic nanoparticles and ions in the environment. TRAC-Trend Anal Chem 75:183–196
13. Zhang XQ, Yin LH, Tang M, Pu YP (2011) ZnO, SiO_2 and Al_2O_3 nanoparticles-induced toxic effects on human fetal lung fibroblasts. Biomed Environ Sci 24(6):661–669
14. Alshatwi AA, Subbarayan PV, Ramesh E, Al-Hazzani AA, Alsaif MA, Alwarthan AA (2012) Al_2O_3 nanoparticles induce mitochondria-mediated cell death and upregulate the expression of signaling genes in human mesenchymal stem cells. J Biochem Mol Toxic 26:469–476
15. Elsayed E, Mahdy A, Sherif F, Hamadeen H (2015) Evaluation of a novel water treatment residual nanoparticles as a sorbent for arsenic removal. J Nanomater 1–10
16. Kim IS, Baek M, Choi SJ (2010) Comparative cytotoxicity of Al_2O_3, CeO_2, TiO_2, and ZnO nanoparticles to human lung cells. J Nanosci Nanotechnol 10:3453–3458
17. Mafuné F, Kohno J, Takeda Y, Kondow T (2011) Dissociation and aggregation of gold nanoparticles under laser irradiation. J Phys Chem B 105:9050–9056
18. Aminfar H (2014) Nanoparticles aggregation in nanofluid flow through nanochannels: insights from molecular dynamic study. Int J Mod Phys C 25(11):1–23
19. Sorokina ON, Kovarski AL, Lagutina MA, Dubrovskii SA, Dzheparov FS (2012) Magnetic nanoparticles aggregation in magnetic gel studied by electron magnetic resonance (EMR). Appl Sci 2:342–350
20. Lehn RCV, Atukorale PU, Carney RP, Yang Y, Stellacci F, Irvine DJ, Alexander-Katz A (2013) Effect of particle diameter and surface composition on the spontaneous fusion of monolayer-protected gold nanoparticles with lipid bilayers. Nano Lett 13:4060–4067
21. Clemments AM, Botella P, Landry CC (2015) Protein adsorption from biofluids on silica nanoparticles: corona analysis as function of particle diameter and porosity. Appl Mater Interfaces 7:21682–21689
22. He YT, Wan J, Tokunaga T (2008) Kinetic stability of hematite nanoparticles: the effect of particle sizes. J Nanopart Res 10:321–332
23. Wu D, Mao F, Yang Z, Wang S, Zhou Z (2014) Silicon and aluminum co-doping of titania nanoparticles: effect on thermal stability, particle size and photocatalytic activity. Mat Sci Semicon Proc 23:72–77
24. Alshammari A, Köckritz A, Kalevaru VN, Martin A (2010) Influence of precursor on the particle size and stability of colloidal gold nanoparticles. Stud Surf Sci Catal 175:409–412
25. Guo Z, Chen G, Zeng G, Liang J, Huang B, Xiao Z, Yi F, Huang Z, He K (2016) Determination of inequable fata and toxicity of Ag nanoparticles in a Phanerochaete chrysosporium biofilm system through different sulfide sources. Environ Sci: Nano 5:1027–1035
26. Saito Y, Shimomura M, Yabu H (2013) Dispersion of Al_2O_3 nanoparticles stabilized with mussel-inspired amphiphilic copolymers in organic solvents and formation of hierarchical porous films by the breath figure technique. Chem Comm 49(54):6081
27. Tan L, Tan X, Fang M, Yu Z, Wang X (2018) Effects of humic acid and Mg^{2+} on morphology and aggregation behavior of silica aerogels. J Mol Liq 264:261–268
28. Pakrashi S, Dalai S, Sneha B, Chandrasekaran N, Mukherjee A (2012) A temporal study on fate of Al_2O_3 nanoparticles in a fresh water microcosm at environmentally relevant low concentrations. Ecotox Environ Safe 84:70–77
29. Son J, Vavra J, Li Y, Seymour M, Forbes V (2015) Interactions between suspension characteristics and physicochemical properties of silver and copper oxide nanoparticles: a case study for optimizing nanoparticle stock suspension using a central composite design. Chemosphere 124:135–142
30. Uyguner CS, Bekbolet M (2005) Evaluation of humic acid photocatalytic degradation by UV-vis and fluorescence spectroscopy. Catal Today 101:267–274
31. Godnjavec J, Zabret J, Znoj B, Skale S, Veronovski N, Venturini P (2014) Investigation of surface modification of rutile TiO_2 nanoparticles with SiO_2/Al_2O_3 on the properties of polyacrylic composite coating. Prog Org Coat 77:47–52
32. Bi Z, Li K, Jiang C, Zhang J, Ma S (2011) Effects of amphoteric oxide (Al_2O_3 and B_2O_3) on the structure and properties of SiO_2-CaO melts by molecular dynamics simulation. J Non-Cryst Solids 559:120687
33. Fairhurst AJ, Warwick P (1998) The influence of humic acid on europium-mineral interactions. Colloid Surface A 145:229–234
34. Chen WP, Chi FH (2002) A study of coagulation mechanism of polyferric sulfate reacting with humic acid using fluorescence-quenching method. Water Res 36(18):4583–4591
35. Chen C, Wang X, Jiang H, Hu W (2007) Direct observation of macromolecular structures of humic acids by AFM and SEM. Colloid Surf A 302:121–125
36. Omar FM, Aziz HA, Stoll S (2014) Aggregation and disaggregation of ZnO nanoparticles: influence of pH and adsorption of Suwannee River humic acid. Sci Total Environ 468–469:195–201
37. Wang Y, Luo X, Han Y, Liu B, Hu Y, Liu X (2020) Preparation of monodisperse polymer particle via in situ charge neutralization-controlled particle coagulation mechanism in macroemulsion polymerization. Colloid Surface A 587:124345
38. Tan L, Tan X, Mei H, Ai Y, Sun L, Zhao G, Hayat T, Alsaedi A, Chen C, Wang X (2018) Coagulation behavior of humic acid in aqueous solutions containing Cs^+, Sr^{2+} and Eu^{3+}: DLS, EEM and MD simulations. Environ Pollut 236:835–843
39. Slade WH, Boss E, Russo C (2011) Effects of particle aggregation and disaggregation on their inherent optical properties. Opt Express 19(9):7945
40. Loosli F, Coustumer PL, Stoll S (2013) TiO_2 nanoparticles aggregation and disaggregation in presence of alginate and Suwannee River humic acids. pH and concentration effects on nanoparticle stability. Water Res 47:6052–6063
41. Wang H, Qi J, Keller AA, Zhu M, Li F (2014) Effects of pH, ionic strength and humic acid on the removal of TiO_2 nanoparticles from aqueous solution phase by coagulation. Colloid Surface A 450:161–165
42. Chen KL, Elimelech M (2007) Influence of humic acid on the aggregation kinetics of fullerene (C_{60}) nanoparticles in monovalent and divalent electrolyte solutions. J Colloid Interf Sci 309:126–134
43. Tan L, Tan X, Fang M, Wang X, Wang J, Xing J, Ai Y, Wang X (2019) Systematic studies on the binding of metal ions in aggregates of humic acid: aggregation kinetics, spectroscopic analyses and MD simulations. Environ Pollut 246:999–1007
44. Engebretson RR, Wandruszka RV (1998) Kinetic aspects of cation-enhanced aggregation in aqueous humic acids. Environ Sci Technol 32(4):488–493
45. Tan L, Tan X, Wang X, Feng J, Fang M, Ai Y, Hayat T, Sun L, Wang X (2019) Effect of co-existing Co^{2+} ions on the aggregation of humic acid in aquatic environment: aggregation kinetics, dynamic properties and fluorescence spectroscopic study. Sci Total Environ 674:544–553
46. Yang K, Chen B, Zhu X, Xing B (2016) Aggregation, adsorption, and morphological transformation of graphene oxide in aqueous

solutions containing different metal cations. Environ Sci Technol 50:11066–11075

47. Raza G, Amjad M, Kaur I, Wen D (2016) Stability and aggregation of titania nanomaterials under environmentally realistic conditions. Environ Sci Technol 50:8462–8472
48. Chen W, Habibul N, Liu XY, Sheng GP, Yu HQ (2015) FTIR and synchronous fluorescence heterospectral two-dimensional correlation analyses on the binding characteristics of copper onto dissolved organic matter. Environ Sci Technol 49:2052–2058
49. Conte P, Piccolo A (1999) Conformational arrangement of dissolved humic substances. Influence of solution composition on association of humic molecules. Environ Sci Technol 33:1682–1690
50. Kalinichev AG, Iskrenova-Tchoukova E, Ahn W, Clark MM, Krikpatrick RJ (2011) Effect of Ca^{2+} on supramolecular aggregation of natural organic matter in aqueous solutions: a comparison of molecular modeling approaches. Geoderma 169:27–32

Publisher's Note Springer Nature remains neutral with regard to jurisdictional claims in published maps and institutional affiliations.

Springer Nature or its licensor (e.g. a society or other partner) holds exclusive rights to this article under a publishing agreement with the author(s) or other rightsholder(s); author self-archiving of the accepted manuscript version of this article is solely governed by the terms of such publishing agreement and applicable law.